

SCIENTIFIC REPORTS



OPEN

Exploiting dispersion of higher-order-modes using M-type fiber for application in mid-infrared supercontinuum generation

D. Jain^{1,5}, C. Markos^{1,2,4}, T. M. Benson², A. B. Seddon² & O. Bang^{1,3,4}

M-type fibers have the exceptional property that the higher-order LP_{0n} modes are core-confined and easily excited, while the LP₀₁ and other modes are confined to a high-index ring surrounding the core, so they are not easily excited. This has profound consequences for mid-infrared supercontinuum sources, where the high zero-dispersion wavelength of chalcogenide and ZBLAN fibers means that exotic pump sources have so far been necessary. We show here that in chalcogenide and ZBLAN M-type fibers the lower ZDW of the core-confined higher-order LP₀₂ mode can be in the range of 2 to 3 μm (around 1.55 μm), while the fiber still has a large core diameter and thus supports high average power. This will allow established pump laser technology to be used in future high-power mid-infrared supercontinuum sources.

Optical fibers have revolutionized human life via their utility in several applications, such as communication, sensing, light sources, and medical equipment etc. Most of the properties of an optical fiber depend on its refractive index profile (RIP). There are different types of optical fibers categorized according to their RIP, such as the standard step-index fiber (SIF), graded-index fiber (GIF), and photonic crystal fiber (PCF). The M-type optical fiber is another fiber with a distinct RIP, which is perhaps not so well-known, even though it has exceptional properties^{1,2}. Figure 1 presents the RIP of an M-type fiber, which has an additional high index ring with thickness *t* surrounding the core of a conventional SIF. Due to the shape of the RIP, resembling the letter “M”, the fiber has become known as the M-type fiber, similar to a W-type fiber¹.

The M-type fiber has special properties, which can be useful for several applications, where standard fibers have limited use. M-type fibers with rather broad rings (large *t*) and shallow refractive index dips (small *dn*) have been exploited in the past for high-power laser applications thanks to their flat fundamental mode profile^{3–5}. This flat (top-hat) profile leads to a dramatic increase in effective mode area^{3–5}, which is useful in avoiding non-linear effects. More recently, M-type fibers with narrow rings (small *t*) and larger refractive index dips (large *dn*) were shown to be suitable for exciting higher-order modes (HOMs) such as the LP₀₂, as core-confined modes, while confining the LP₀₁ and other modes to the high index ring, so that they are not easily excited^{6–11}. Using an extra refractive index structure in the form of a depressed cladding region it was shown that using the core-confined LP₀₂ mode the zero-dispersion wavelength (ZDW) could be pushed below 1 μm in a silica fiber⁸. It was further stated that had the core index and the index of the ring been significantly higher than that of silica, then the extra depressed cladding structure would not have been necessary⁸.

The main scope of this paper is to explore the M-type fiber design for shifting the ZDW of non-silica fibers, like chalcogenide and ZBLAN fibers, towards shorter wavelengths for application in mid-infrared (IR) supercontinuum (SC) generation. It is pertinent to note that mid-IR wavelength is extremely useful wavelength region as several chemical compounds and molecules display unique and strong mid-IR spectral finger prints in this region. Recently, mid-IR fiberized SC sources have shown their utility in different application such as Optical Coherence Tomography¹², Tissue Imaging¹³, and as an alternative option of Synchrotrons¹⁴.

¹DTU Fotonik, Department of Photonics Engineering, Technical University of Denmark, Lyngby, Denmark. ²George Green Institute for Electromagnetics Research, University of Nottingham, Nottingham, NG7 2RD, UK. ³NKT Photonics A/S, Blokken 84, 3460, Birkerød, Denmark. ⁴NORBLIS IVS, Virumgade 35D, 2830, Virum, Denmark. ⁵School of Physics and The University of Sydney Nano Institute, The University of Sydney, Sydney, NSW, 2006, Australia. Correspondence and requests for materials should be addressed to D.J. (email: deepak.jain@sydney.edu.au)

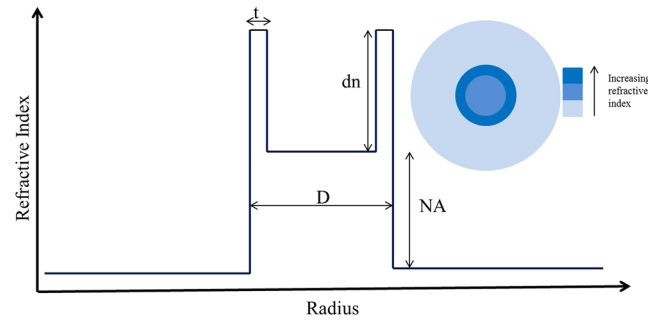


Figure 1. Refractive index profile of the M-type fiber with characteristic parameters t , dn , D , and NA . The inset shows the end facet of an M-type fiber.

It is most efficient to pump the fiber near the ZDW for SC generation^{15,16}. However, the ZDW of a material is fixed, so, in order to match it with available pump sources, a strong additional contribution from waveguide dispersion is generally required. Today's SC sources use a silica PCF to provide the required ZDW and tight confinement, but silica PCFs are difficult to fabricate as they involve a complex stack and draw process and fiber handling (such as cleaving and splicing) is difficult due to the presence of air-holes¹⁷. Furthermore, it is even more challenging to fabricate PCFs based on chalcogenide^{18,19} and in particular ZBLAN glasses^{20,21} that are required for mid-IR SC sources²².

Even if the PCF technology can be matured the chalcogenide and ZBLAN glasses have such a long material ZDW that moving the ZDW sufficiently down to for example $1.5\ \mu\text{m}$ to use Erbium pump lasers required so small cores that power handling becomes a critical issue²³. Chalcogenide SIFs can be made with a very high NA above 1, but the dispersion of their fundamental LP_{01} mode is nevertheless not appropriate for broadband SC generation²⁴.

An answer to the problems could be to use the M-type fiber and the fact that HOMs in conventional SIFs, such as the LP_{02} and LP_{03} modes, have a shorter ZDW than the LP_{01} mode^{25,26}. As stated above it is possible to excite the LP_{02} or LP_{03} mode in an M-type fiber, while confining major fraction of power of the lower order modes (LOMs) such as LP_{01} , LP_{11} , and LP_{21} to the ring only. In this paper, we therefore explore the properties of M-type fibers providing a short ZDW in large-core SIFs for optimum SC generation. To the best of our knowledge, this is the first report showing the potentially very advantageous use of an M-type fiber in high-power SC generation in general and mid-IR SC generation in particular.

Working Principle of the M-type Fiber

Figure 1 shows the RIP of the M-type fiber and the notations used in this paper: D is the core diameter, t is the thickness of the high-index ring, NA is the numerical aperture (NA) of the core with respect to the cladding, and dn is the refractive index difference between the high index ring and the core.

The working principle of an M-type fiber is different from a conventional SIF due to the different RIP. The special M-type RIP brings two features to an M-type fiber. The first one is how the spatial distribution of the modes varies with wavelength. The second one is the hybrid guiding mechanism consisting of both total internal reflection and anti-resonance guidance (similar to bandgap guidance). In an M-type fiber, the spatial distribution of the mode varies dramatically with wavelength, hence it is possible to confine the major power fraction of LP_{0n} modes to the core, while the major power of LP_{01} mode and other modes are confined to the ring. Numerical simulations on these fibers have been performed with the full-vectorial finite element method (FEM) based software "COMSOL". However, scalar LP notations have been used to follow conventional notations as the index difference between core and cladding is not high enough to cause any considerable difference. For dispersion calculations of LP_{01} and LP_{02} modes, a perfect degeneracy for both orthogonal polarizations has been assumed.

Figure 2(a) shows the RIP of a SIF and Fig. 2(b) shows the calculated total dispersion of the LP_{01} and LP_{02} modes, for two different fibers with core diameter $D = 12\ \mu\text{m}$ and $NA = 1$ and 1.8 . Here we used two glasses composed of $As_{40}Se_{60}$ (n_1) and $Ge_{10}As_{23.4}Se_{66.6}$ (n_2), respectively, whose refractive indices were obtained from the refractive index measurement reported in²⁷. The Sellmeier equations used in our studies are:

$$n_1^2 = 1 + \frac{6.558\lambda^2}{\lambda^2 - 0.09456} + \frac{0.8558\lambda^2}{\lambda^2 - 1669} + \frac{0.08432\lambda^2}{\lambda^2 - 0.5489} \quad (1)$$

$$n_2^2 = 1 + \frac{0.2325\lambda^2}{\lambda^2 + 0.3793} + \frac{0.8622\lambda^2}{\lambda^2 - 1709} + \frac{5.435\lambda^2}{\lambda^2 - 0.1036} \quad (2)$$

We consider SIFs composed of a core material with $n_{\text{core}} = n_1$ and a cladding material with $n_{\text{clad}} = n_2$, which at $3\ \mu\text{m}$ has an NA of ~ 0.99 , calculated from the standard relation:-

$$NA^2(\lambda) = n_1^2(\lambda) - n_2^2(\lambda) \quad (3)$$

This is termed the $NA=1$ SIF and is the fiber used in²⁸. However, we need several different NAs to observe the impact of NA on the ZDW. In order to increase the NA, we decreased the refractive index of the cladding by a factor independent of wavelength:-

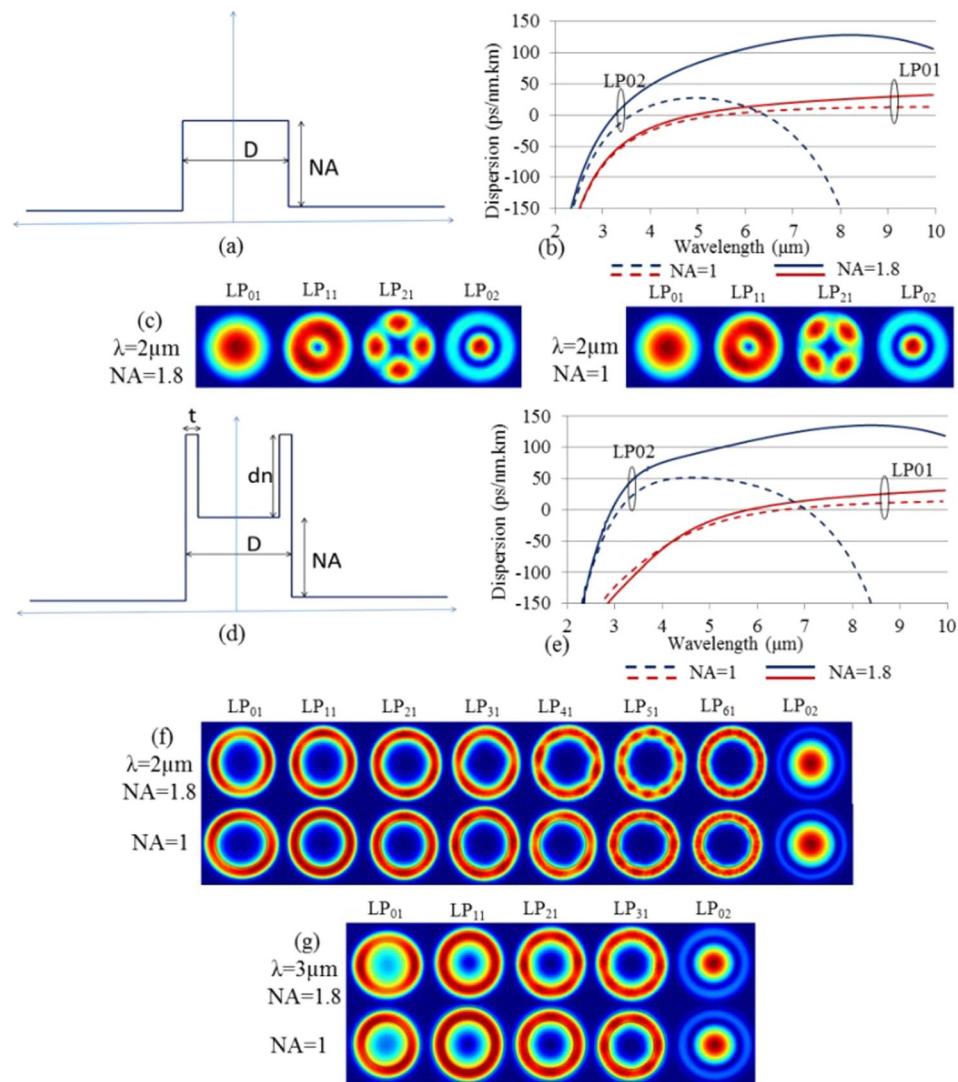


Figure 2. (a) Refractive index profile of a SIF, (b) calculated dispersion of the LP₀₁ and LP₀₂ modes of two chalcogenide SIFs with $D = 12 \mu\text{m}$ and $NA = 1$ and 1.8 , respectively, (c) electric field intensity profile at $\lambda = 2 \mu\text{m}$ of guided modes in the SIFs, (d) RIP profile of an M-type fiber, (e) calculated dispersion of the LP₀₁ and LP₀₂ modes of two chalcogenide M-type fibers with $D = 12 \mu\text{m}$, $dn = 0.05$, $t = 2 \mu\text{m}$, and $NA = 1$ and 1.8 , respectively, (f) electric field intensity profile of guided modes at $\lambda = 2 \mu\text{m}$, and (g) electric field intensity profile of guided modes at $3 \mu\text{m}$ for both M-type fibers.

$$NA^2(\lambda) = n_1^2(\lambda) - (n_2(\lambda) - X)^2 \quad (4)$$

Figure 2(c) shows the electric field intensity profile of various modes of $NA = 1$ and 1.8 SIFs. In order to extend this study to an M-type fiber, we modified the SIF to an M-type fiber with the same basic parameters by increasing the index by $dn = 0.05$ in a small outer ring of thickness $t = 2 \mu\text{m}$ of the core of the SIF (c.f. Fig. 2(d)). The core diameter and NA is the same for the two fiber types ($D = 12 \mu\text{m}$ and $NA = 1$ or 1.8) and the new additional parameters are fixed at $t = 2 \mu\text{m}$ and $dn = 0.05$. We obtained the refractive index of the high index ring as $n_{\text{ring}}(\lambda) = n_1(\lambda) + dn$. Figure 2(e) shows the calculated dispersion of the M-type fibers for the LP₀₁ and LP₀₂ modes within the same wavelength range as before. Figure 2(f,g) show the electric field intensity profile of several guided modes at 2 and $3 \mu\text{m}$ wavelengths for both fibers, respectively.

It is evident that the first mode residing in the central core region is the LP₀₂ mode for both M-type fibers with $NA = 1.8$ and 1 . Hence, it is possible to excite the LP₀₂ mode while avoiding the modes residing primarily in the ring. In this way, one can exploit the ZDW of the LP₀₂ mode ($3.14 \mu\text{m}$ and $2.94 \mu\text{m}$ for $NA = 1$ and 1.8 , respectively), which is much shorter than the ZDW of the LP₀₁ mode ($6.59 \mu\text{m}$ and $5.81 \mu\text{m}$ for $NA = 1$ and 1.8 , respectively) as shown in Fig. 2(e). It is important to note that, for a SIF with the same core diameter $D = 12 \mu\text{m}$ with $NA = 1$ and 1.8 , the ZDW of the LP₀₁ mode is also much higher at $5.48 \mu\text{m}$ and $4.9 \mu\text{m}$, respectively, as shown in Fig. 2(b).

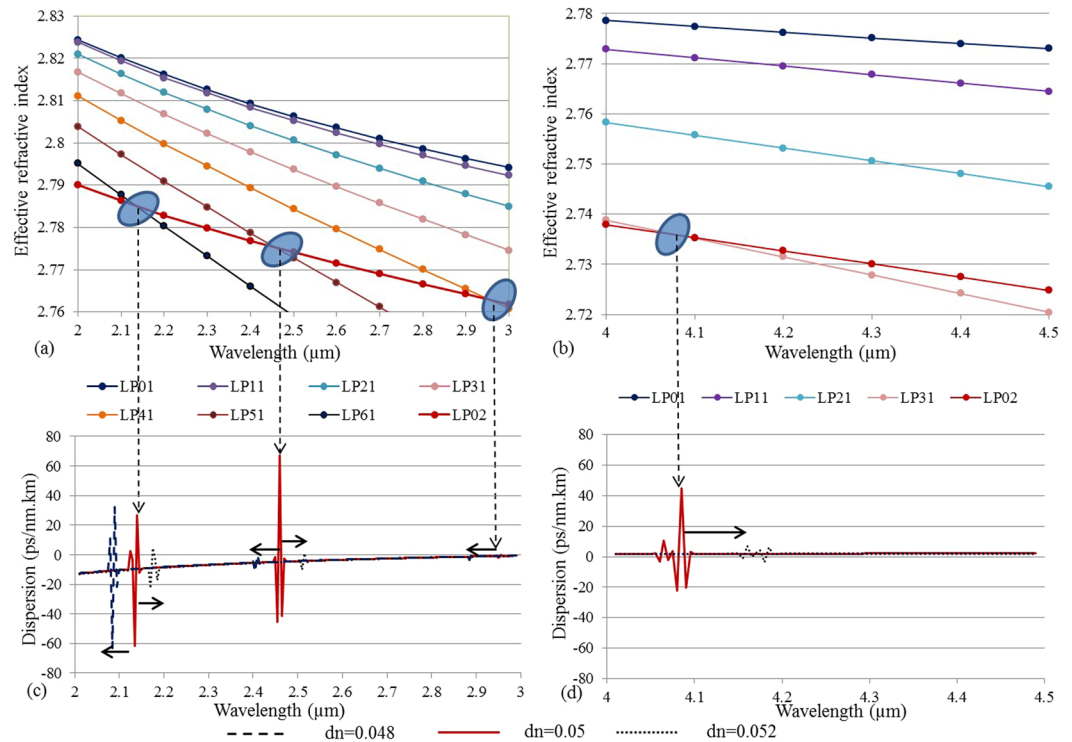


Figure 3. Variation of the effective refractive indices with respect to wavelength of several modes of the chalcogenide M-type fiber. (a) shows resonant coupling between the LP_{02} mode and the LP_{61} , LP_{51} , and LP_{41} modes, (b) shows resonant coupling between LP_{02} and LP_{31} . The core diameter (D) is $12\ \mu\text{m}$, ring thickness (t) is $2\ \mu\text{m}$, NA is 1, and dn is 0.05. (c) and (d) shows the calculated dispersion of the LP_{02} mode for different dn . Still $D = 12\ \mu\text{m}$, $t = 2\ \mu\text{m}$, and $NA = 1$.

Figure 3(a,b) shows the variation of the effective refractive index of different modes of an M-type fiber ($D = 12\ \mu\text{m}$, $NA = 1$, $t = 2\ \mu\text{m}$, and $dn = 0.05$). With increasing wavelength, the effective refractive indices of the LP_{61} , LP_{51} , LP_{41} , and LP_{31} modes rapidly decrease and cross the LP_{02} mode leading to resonant coupling at the specific wavelengths. This leads to local fluctuations in the dispersion profile of the LP_{02} mode as shown in Fig. 3(c,d), which may have implications for the SC generation. The similar resonant couplings effects were observed in silica photonic bandgap fiber⁶ and silica M-type fiber¹¹. In fact, in silica M-type fiber the effect was exploited for pulse compression¹¹. It is therefore important that one can shift these crossings by varying the fiber parameters. If one for example changes dn of the ring while keeping all other parameters to be the same then this changes the effective refractive indices of the modes in the ring and shifts the resonant coupling wavelength between these ring-confined modes and the LP_{02} mode, as seen in Fig. 3(c,d). Decreasing (increasing) dn by 0.002 for example shifts the $2.14\ \mu\text{m}$ resonance by $0.05\ \mu\text{m}$ ($0.035\ \mu\text{m}$). Studying how these narrow-band crossings influence the SC generation will be the subject of future investigations, here we limit ourselves to a thorough study of the mode properties and dispersion.

Figure 4 explores these couplings in detail by showing the profile of the electric field intensity of the modes at different wavelengths close to the crossing. Away from the crossing the modes are all radially symmetric and therefore not orthogonal, which means that they couple strongly close to the crossing. Resonant coupling is thus clearly observed, which confirms a guiding mechanism similar to that found in photonic bandgap fibers (PBGFs), although total internal reflection guidance dominates^{8,29}. It is pertinent to note that because there is only one resonator (the high-index ring) the couplings encountered here are weak and occur only in a 10–20 nm bandwidth. In a PBGF there are several resonators (in all-solid PBGFs these are, e.g., the high-index regions) and the mutual coupling between the same mode of these many resonators leads to the formation of the broader bands³⁰.

Chalcogenide M-type Fibers

The investigations in the previous section have revealed the potential of M-type fibers for utilizing the LP_{02} mode for obtaining a core-guided mode with a shorter ZDW. In order to optimize and understand the advantage of M-type fibers over SIFs, it is important to do a comparative analysis of the first ZDWs (F-ZDWs) and second ZDWs (S-ZDWs) of M-type and SIFs with the same core diameters and NAs. Figure 5 shows a plot of the F-ZDW and S-ZDW of chalcogenide SIFs for different core diameter and NAs. The material dispersion given in Eqs (1–2) has been taken into account. In order to increase the NA, we again decreased the refractive index of the cladding by a factor independent of wavelength $NA(\lambda)^2 = n_1(\lambda)^2 - (n_2(\lambda) - X)^2$ as mentioned in Section 2. It is important to understand that the NAs considered here are practically achievable and have been successfully fabricated^{27,28,31,32}.

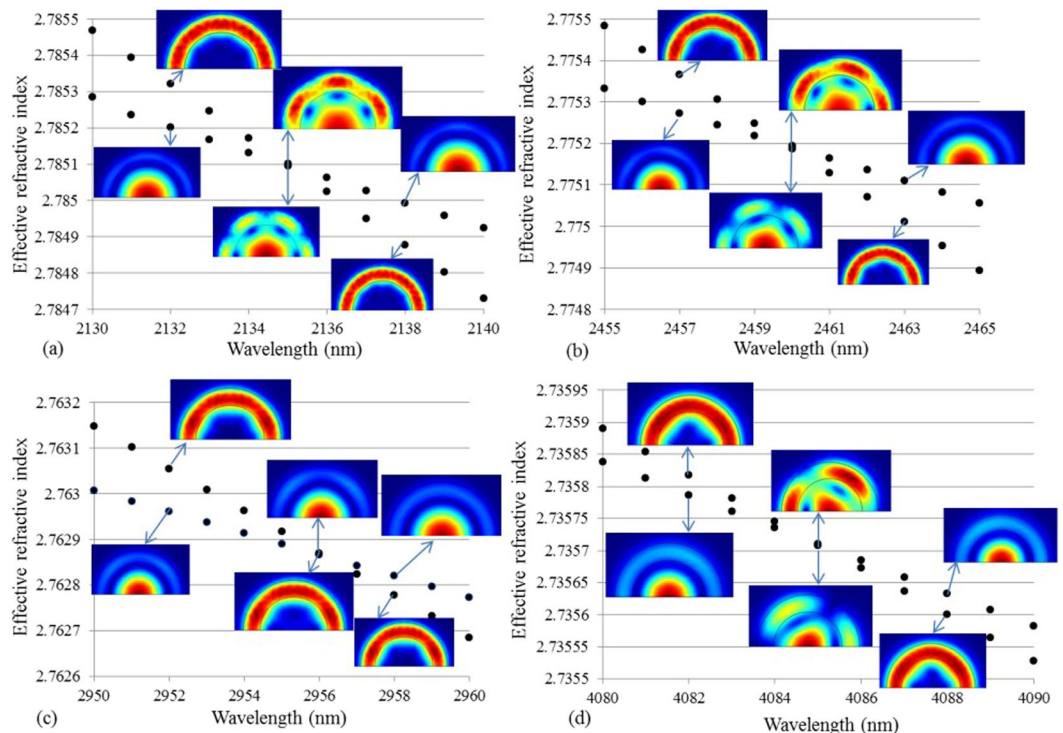


Figure 4. Variation of the effective refractive indices and profile of the electric field intensity for different couplings encountered by the LP₀₂ mode in the chalcogenide M-type fiber. (a) LP₆₁ and LP₀₂, (b) LP₅₁ and LP₀₂, (c) LP₄₁ and LP₀₂, and (d) LP₃₁ and LP₀₂. The core diameter (D) is 12 μm , ring thickness (t) is 2 μm , NA is 1, and dn is 0.05.

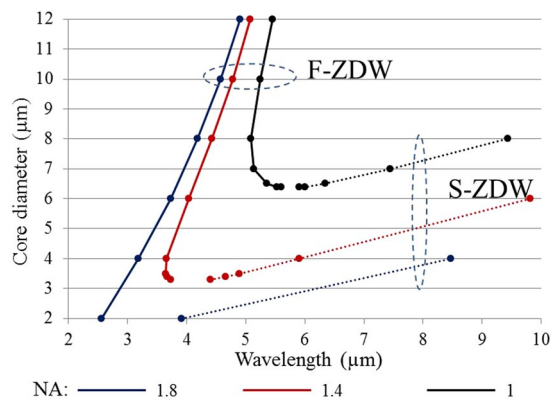


Figure 5. F-ZDW (solid curves) and S-ZDW (dotted curves) versus core diameter for the fundamental mode (LP₀₁) of a conventional chalcogenide SIF for different NAs.

It is interesting to observe the trends in Fig. 5, with increasing core diameter F-ZDW and S-ZDW generally increase and a significant increase in the bandwidth (BW) with anomalous dispersion, defined as $BW = (F-ZDW) - (S-ZDW)$, can be observed. Similarly, when increasing NA for a fixed core diameter, the F-ZDW decreases and the S-ZDW increases, which again leads to an increase in BW. In order to shift the F-ZDW to shorter wavelength, it is desirable to have a large NA and small core diameter thanks to the strong guidance of the light. However a combination of large NA and small core diameter leads to very small BW not suitable for broadband SC generation; moreover a small core diameter leads to reduced coupling efficiency and poor power handling. Based on Fig. 5 we can conclude that the F-ZDW remains higher than 5 μm and 3.6 μm for NAs of 1 and 1.4, respectively, irrespective of core diameter. In contrast, for an ultra-high NA of 1.8, the F-ZDW can be shifted below 3 μm for core diameters below 3.4 μm . However, due to the generic variation of the ZDWs, the bandwidth is significantly degraded for core diameters below 3 μm , with the S-ZDW even being below the 4.5 μm loss edge of ZBLAN fibers, thereby taking away all the advantages of long wavelength guidance of chalcogenide fibers.

The above investigation verifies the limitation of using SIFs to achieve a dispersion profile suitable for broadband mid-IR SC generation using established ytterbium, erbium, and thulium pump laser technologies. Even

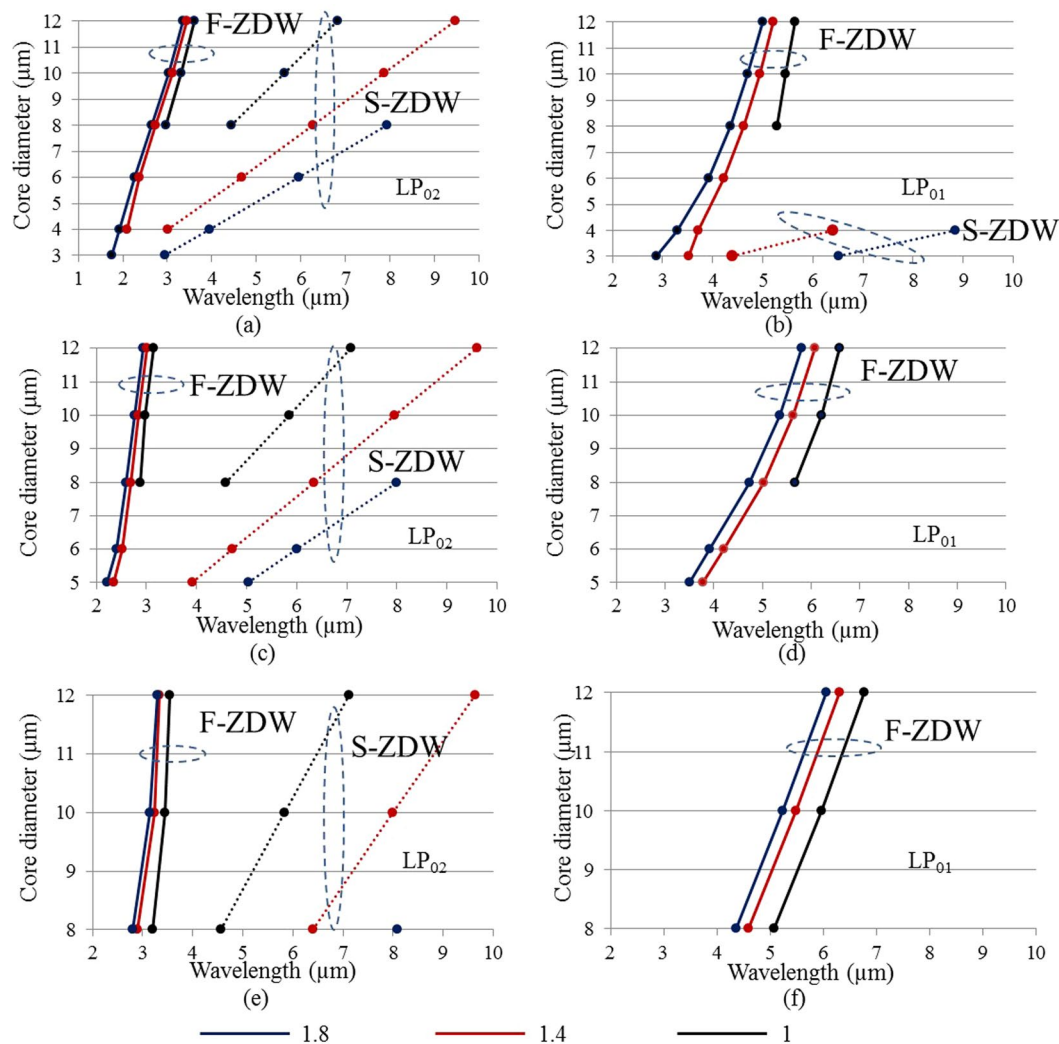


Figure 6. F-ZDW (solid curves) and S-ZDW (dashed curves) versus core diameter for the LP₀₂ and LP₀₁ mode of an M-type chalcogenide fiber for different NAs and ring thicknesses, while $dn = 0.05$ is fixed. M-type fiber demonstrated in (a–d), and (e,f) have $t = 1 \mu\text{m}$, $t = 2 \mu\text{m}$, and $t = 3 \mu\text{m}$, respectively.

the emerging Er:ZBLAN fiber laser technology at $2.8 \mu\text{m}$ seems to be useless as a pump source³³. Therefore, it is desirable to improve the fiber design in order to at the same time have a larger core diameter and a shorter first ZDW, so that coupling efficiency and power handling can be increased.

The goal is to shift the first ZDW to be below $2 \mu\text{m}$ in order to employ mature fiber laser technology or at least below $2.94 \mu\text{m}$ to use Er:ZBLAN fiber lasers³³. However, any improvement in fiber design pushing down the ZDW of large core diameter chalcogenide fibers, will in fact be helpful. Figure 6 considers M-type fibers and shows the calculated F-ZDW and S-ZDW of the LP₀₁ and LP₀₂ modes for different D , t , and NA, but with dn fixed at 0.05. Figure 6(a–f) show the F-ZDW and S-ZDW of the LP₀₁ and LP₀₂ modes for $t = 1 \mu\text{m}$, $2 \mu\text{m}$, and $3 \mu\text{m}$ respectively. A comparison of Figs 5, 6 shows the significantly shorter F-ZDW of the M-Type LP₀₂ mode compared to the F-ZDW of the LP₀₁ mode of a conventional SIF for all NAs and core diameters. The F-ZDW of the M-type fiber varies from 1.92 to $3.6 \mu\text{m}$ for all core diameters from $4 \mu\text{m}$ to $12 \mu\text{m}$ and NAs from 1 to 1.8. On the other hand the F-ZDW of a SIF varies from $3.2 \mu\text{m}$ to $5.5 \mu\text{m}$ for core diameters from $4 \mu\text{m}$ to $12 \mu\text{m}$ and NAs from 1 to 1.8. In addition to shifting the F-ZDW towards shorter wavelengths, another benefit arises as the larger core of the M-type fiber affords more pump power handling capacity. Figure 6 shows the dramatic improvement offered by the M-type fiber in shifting down the ZDW of a corresponding SIF with the same core diameter and NA by more than 1500 nm . Considering only core diameters above $4 \mu\text{m}$ for good power handling, we see that in fact even for the M-type fiber, no combinations of $D \geq 4 \mu\text{m}$, $NA \leq 1.8$, and $t \geq 1 \mu\text{m}$ allows a broad mid-IR SC by directly pumping with a $2 \mu\text{m}$ laser in the anomalous dispersion regime above the F-ZDW in a fiber with a S-ZDW larger than $6 \mu\text{m}$. However, the M-type fibers do open the door for direct pumping by a $2.94 \mu\text{m}$ Er:ZBLAN fiber laser³³. Figure 7 shows the F-ZDW versus the ring thickness t for different core diameters, NAs, and dn . We see that there seems to be an optimum value of t around $= 2 \mu\text{m}$ at which the F-ZDW is a minimum and below $2.9 \mu\text{m}$ for all parameter combinations, which is suitable for using an Er:ZBLAN fiber pump laser. It is important that that for

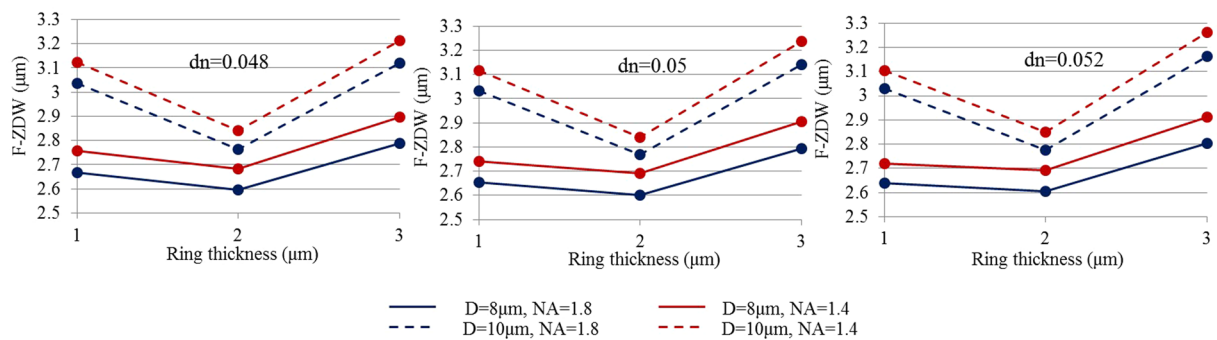


Figure 7. F-ZDW versus ring thickness for different core diameters (8 μm and 10 μm) and NAs (1.4 and 1.8) for varying dn (a) dn = 0.048, (b) dn = 0.05, and (c) dn = 0.052.

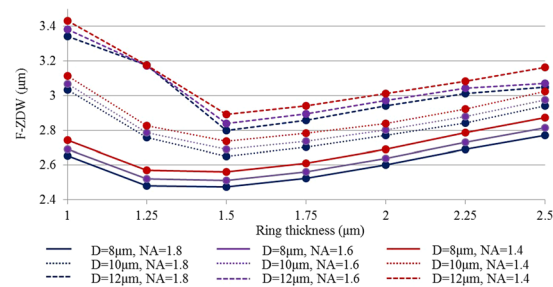


Figure 8. F-ZDW versus ring thickness for different core diameters (8 μm, 10 μm, and 12 μm) and NAs (1.4, 1.6, and 1.8) for fixed dn = 0.05.

$t = 2 \mu\text{m}$ even for a large core diameter of 10 μm and an NA of 1.4, which is achievable today³¹, the M-type fiber has an F-ZDW below 2.9 μm.

In order to further zoom in on the optimum parameters with a minimum of F-ZDW and maximum S-ZDW, we performed more simulations. Figure 8 shows the F-ZDW for different ring thicknesses between 1 and 2.5 μm, core diameters $D = 8, 10,$ and $12 \mu\text{m}$, and NA = 1.4, 1.6, and 1.8. In Fig. 8, we did not investigate the impact of the dn variation, as Fig. 7 already showed the negligible impact of a change in dn from 0.048 to 0.052 had on the F-ZDW. Figure 8 shows that the minimum is closer to $t = 1.5 \mu\text{m}$ and that the F-ZDW remains lower than 3 μm for most of the fiber parameters, thereby ensuring a possibility to be pumped by a 2.94 μm laser. In terms of the S-ZDW, it remained longer than 7.92 μm for $t \geq 1.5 \mu\text{m}$ and all parameters other than $D = 8 \mu\text{m}$ and NA = 1.4 and 1.6. In order to achieve a broadband spectrum, it is good to look for parameters fulfilling the following conditions: $F\text{-ZDW} \leq 3$ and $S\text{-ZDW} \geq 7.9 \mu\text{m}$. The following sets of parameters out of the parameters shown in Fig. 8 fulfil these conditions, (1) $D = 8 \mu\text{m}$, NA = 1.8, irrespective of t , (2) $D = 10 \mu\text{m}$, irrespective of t and NA other than $t = 1 \mu\text{m} - 1.25 \mu\text{m}$ and NA = 1.4, and (3) $D = 12 \mu\text{m}$, $t = 1.5, 1.75,$ and $2 \mu\text{m}$, and irrespective of NA.

The optimum M-type fiber design considered here with an F-ZDW of 2.6 μm can in fact be pumped with a 2 μm broadband laser by using in-amplifier supercontinuum generation^{34,35}. Recently, high power SC sources extending up to ~2.7 μm in all-fiber thulium doped fiber amplifier (TDFA) have been reported³⁶. Further, SC sources extending up to 3.2 μm in a Germania doped silica fiber have also been achieved by pumping with a 1550 nm laser source in an all-fiber configuration^{37,38}. In particular the latter could be promising to pump most of the M-Type fibers shown in Fig. 8. In recent years, a cascaded pumping scheme has also emerged as a versatile tool to compensate for the unavailability of fiber lasers above 2 μm^{36,39,40}. A typical example of cascaded pumping of chalcogenide fibers in mid-IR SC generation is pumping first a ZBLAN fiber using a conventional 2 μm laser and then couple the supercontinuum output of the ZBLAN fiber (normally extending up to ~4.2 μm) into a chalcogenide fiber for further broadening. It is quite obvious that a SIF may not be an exciting option in this cascaded configuration due to its stringent trade-off between core diameter, short F-ZDW, and large BW as shown in Fig. 5. In a recent experimental study of such cascaded configurations, a suspended core chalcogenide fiber of ~4.5 μm diameter having a ZDW of ~3.5 μm was used, which has limited coupling efficiency due to the small core and very bad power handling capability because the 3 large holes around the core thermally isolates the core⁴⁰. It is very important to make a note here that, there are several other combinations of t and dn having ZDW lower than 3.5 μm being suitable for cascaded configuration. An improved M-type fiber design having a shorter ZDW with a larger core diameter than a SIF will open the door to power scaling in this cascaded scheme, as more power from the ZBLAN fiber output will be in the anomalous dispersion regime of the chalcogenide fiber.

Going deeper into the properties of the M-Type fiber it is extremely important to note that, in order to excite the LP_{02} mode without exciting the LP_{01} and other modes, it is necessary to choose the thickness (t) and the

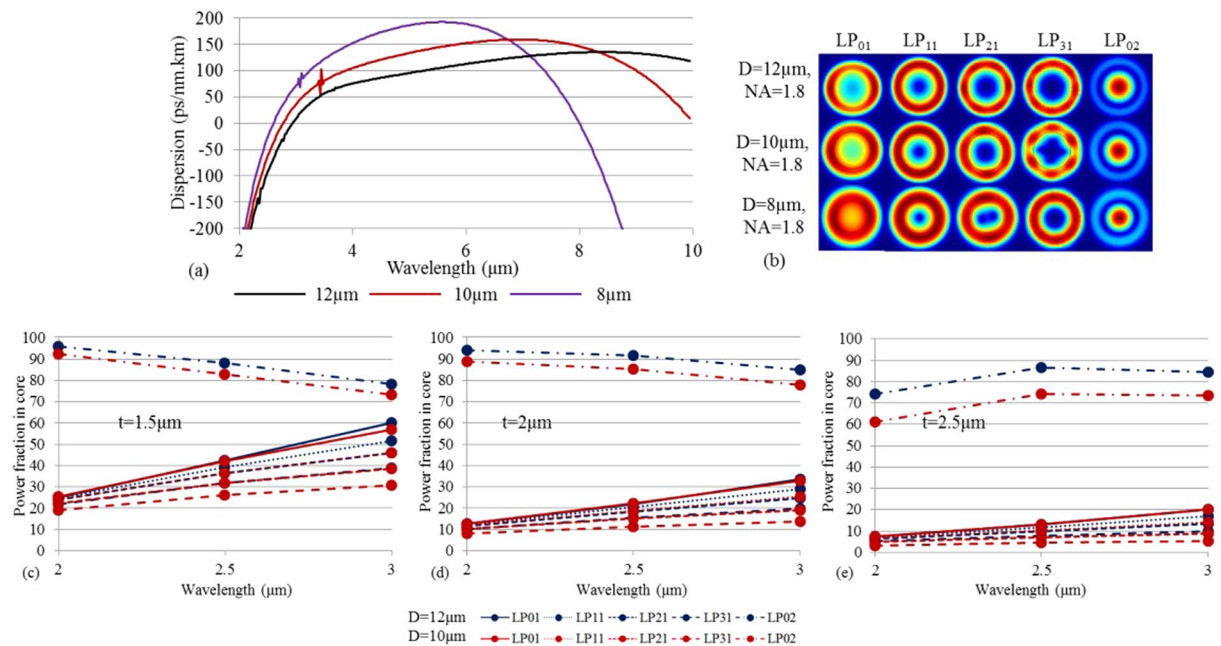


Figure 9. (a) Dispersion versus wavelength for varying core diameter. The other parameters are $t = 2 \mu\text{m}$, $NA = 1.8$, and $dn = 0.05$. (b) The electric field intensity profile of the several modes for different core diameter at $3 \mu\text{m}$ wavelength. (c–e) show the power fraction in core for different modes at different wavelengths for varying t . The other parameters are $NA = 1.8$ and $dn = 0.05$.

refractive index (dn) of the ring, so that all these unwanted modes lie in the high-index ring with much less power in the core than the LP_{02} mode. In Fig. 9 we consider M-type fibers with $NA = 1.8$, $t = 2 \mu\text{m}$, and $dn = 0.05$, and varying core diameters. From the dispersion profiles we again see the narrow-band small spikes in the 2 to $4 \mu\text{m}$ region, originating from the coupling between LP_{31} and LP_{41} modes with the LP_{02} mode. Figure 9(b) shows the profiles of the electric field intensity of various modes for different core diameters at $\lambda = 3 \mu\text{m}$. In particular we see that indeed the LP_{02} mode is core-guided, but we also see that in fact the LP_{01} mode, while still having most power in the ring, is starting to have significant power in the core as the core diameter is decreased from $12 \mu\text{m}$ to $8 \mu\text{m}$. In Fig. 9(c–e) we study this point by plotting the fraction of power in the core of the LP_{02} mode and the main ring-based modes (LP_{01} , LP_{11} , LP_{21} , LP_{31}) for a ring thickness of $t = 1.5 \mu\text{m}$, $2 \mu\text{m}$, and $2.5 \mu\text{m}$, and core diameters of $D = 10 \mu\text{m}$ and $12 \mu\text{m}$. The other parameters are $NA = 1.8$ and $dn = 0.05$. Figure 9(c–e) demonstrates that when the core diameter and ring thickness are sufficiently large then the power of the ring-guided modes in the core is so small that the LP_{02} mode effectively is the only core-guided mode. For the small thickness of $t = 1.5 \mu\text{m}$, however, the power in the core of the ring-guided modes start to become comparable to that of the LP_{02} mode at longer wavelength, which means that significant coupling can be anticipated. Combined with the ZDW investigations it appears that a thickness of $2 \mu\text{m}$ and a core diameter of $10 \mu\text{m}$ is reasonable for $2.9 \mu\text{m}$ pumped broadband mid-IR SC generation.

In view of the beneficial properties of the core-guided LP_{02} mode in the M-type fiber an interesting question could be whether the also core-guided LP_{03} mode could be used to achieve an even shorter F-ZDW. In order to explore this, we further extended the study to a thickness of $t = 3 \mu\text{m}$. Figure 10(a) shows the calculated dispersion for the core-guided LP_{02} and LP_{03} modes for two core diameters $D = 10 \mu\text{m}$ and $12 \mu\text{m}$. The other parameters are: $NA = 1.8$ and $dn = 0.05$. The F-ZDW for the LP_{03} mode is between 2.1 and $2.2 \mu\text{m}$. It is difficult to determine the exact value due to a very strong spike due to coupling with ring modes in this range, much stronger than what has been seen for the LP_{02} mode. Although the LP_{03} mode has much shorter F-ZDW than LP_{02} ($> 3 \mu\text{m}$) but it comes at the cost of a shorter S-ZDW, which is lower than $7.7 \mu\text{m}$ for $D = 12 \mu\text{m}$. Figure 10(b) shows the profile of the electric field intensity of different modes for $D = 12 \mu\text{m}$ and demonstrates that the LP_{02} and LP_{03} modes are core-guided at $\lambda = 2 \mu\text{m}$, while the other modes are ring-guided. At a first look exploiting the LP_{03} mode could seem a tempting option for mid-IR SC generation, as it potentially allows using a $2 \mu\text{m}$ pump laser source. However, the results of Fig. 10 show that the LP_{03} mode suffers more from resonant couplings with ring-guided modes and from a short S-ZDW, than the LP_{02} mode. A detailed investigation would therefore be required to judge the advantages of the LP_{03} mode over the LP_{02} mode. Furthermore, for M-type silica fibers, researchers have used two high index layer in place of one to exploit the LP_{03} modes¹⁰, however it might be fairly difficult to have two high index layers in case of chalcogenide compared to the silica glass based fibers. Therefore, exploitation of LP_{03} using two index layers has been left here for future work.

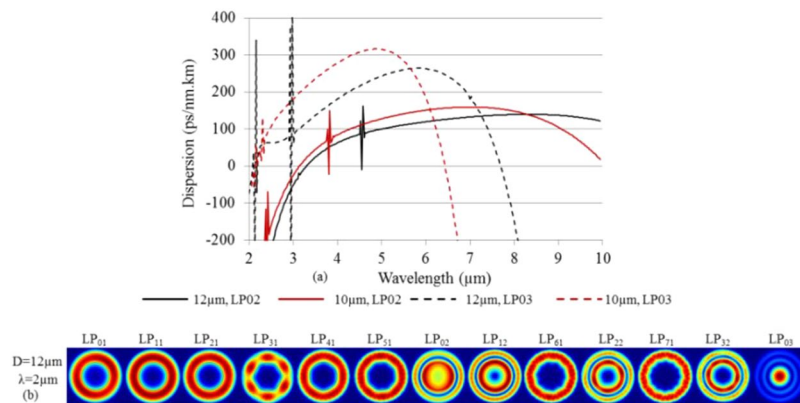


Figure 10. (a) Dispersion of the core-guided modes LP_{02} and LP_{03} modes versus wavelength for two different core diameter. The other parameters are $t = 3 \mu\text{m}$, $NA = 1.8$, and $dn = 0.05$. (b) The electric field intensity profile of several modes for $D = 12 \mu\text{m}$, $t = 3 \mu\text{m}$, $NA = 1.8$, and $dn = 0.05$.

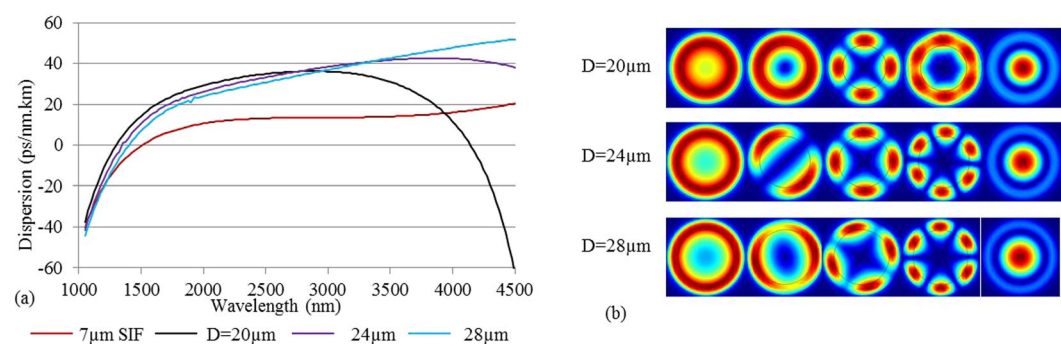


Figure 11. (a) Dispersion profile of the LP_{01} mode of a ZBLAN SIF with $D = 7 \mu\text{m}$ and $NA = 0.3$, and the LP_{02} mode of an M-type ZBLAN fiber with $D = 20 \mu\text{m}$, $24 \mu\text{m}$, and $28 \mu\text{m}$, $t = 4 \mu\text{m}$, $dn = 0.005$, and $NA = 0.3$. (b) The electric field intensity profile of several modes for all three M-type fibers at $1.55 \mu\text{m}$ wavelength.

ZBLAN M-type Fibers

In Fig. 11 we extend the study of M-type fibers to ZBLAN fibers. Here we have assumed a core having the composition $53\%ZrF_4-20\%BaF_2-4\%LaF_3-3\%AlF_3-20\%NaF$, whose refractive index was obtained using the Sellmeier equation reported in⁴¹. We obtained the index of the cladding as $n_{cl}(\lambda)^2 = n_c(\lambda)^2 - NA$ and of the high-index ring as $n_r(\lambda) = n_c(\lambda) + dn$. Figure 11(a) shows the dispersion profile of the LP_{01} mode of a ZBLAN based SIF with $D = 7 \mu\text{m}$ and $NA = 0.3$, and of the LP_{02} mode of three M-type ZBLAN fibers with $D = 20 \mu\text{m}$ to $28 \mu\text{m}$, $t = 4 \mu\text{m}$, $dn = 0.005$, and $NA = 0.3$. Figure 11(b) shows the profile of the electric field intensity at $1.55 \mu\text{m}$ for the M-type fibers with different core diameters ($D = 20 \mu\text{m}$, $D = 24 \mu\text{m}$, and $D = 28 \mu\text{m}$). The mode profiles show that all modes lower than the LP_{02} are confined to the ring, which ensures the excitation of the LP_{02} mode as the fundamental mode is possible. One can further see how the ring-guided modes become increasingly confined to the ring as the core diameter is increased.

Figure 11(a) shows that the ZDW increases with increasing core diameter. It is interesting to note that, the ZDW for none of these fibers exceeds $1.4 \mu\text{m}$; on the contrary a $7 \mu\text{m}$ core diameter SIF with $0.3 NA$ has a ZDW of $1.5 \mu\text{m}$. It is important to keep in mind that, with increasing core diameter, the ZDW will shift to a longer wavelength; hence it can be concluded that a $7 \mu\text{m}$ core diameter (for $NA = 0.3$) is towards the maximum core diameter of a SIF that can be pumped efficiently by a $1.55 \mu\text{m}$ source in the most efficient anomalous dispersion regime. On the contrary, an M-type fiber (with same $NA = 0.3$) has a ZDW lower than $1.5 \mu\text{m}$, even with a core diameter of $28 \mu\text{m}$ (four times larger than the $7 \mu\text{m}$ core SIF). This again shows the clear opportunity of pumping the M-type ZBLAN fiber with a $1.55 \mu\text{m}$ source and using the much larger core to handle more power⁴².

Conclusion

Our results have demonstrated that M-type fibers have tremendous potential for mid-IR supercontinuum generation applications through the capability of having HOMs, such as the LP_{02} or LP_{03} modes as a fundamental mode and consequently having shorter ZDWs with larger core diameters. In case of chalcogenide fibers, the ZDWs can be shifted down into the range of $2 \mu\text{m}$ to $3 \mu\text{m}$ wavelength. The above investigations show the great potential of the M-type fiber to be pumped by a $2.8 \mu\text{m}$ Er:ZBLAN laser, a broadband Tm and Ho doped fiber laser, a highly non-linear Germania doped fiber having broadband supercontinuum spectrum output, and a supercontinuum

output of a ZBLAN fiber. Here, due to the shorter ZDW of the M-type fiber compared to its counterparts such as SIFs or suspended core fibers, more solitons from a supercontinuum pump source (such as a supercontinuum output from ZBLAN fiber) can be pushed into anomalous dispersion leading to more output power towards longer wavelengths. Further investigations revealed the tremendous potential of using a 1.55 μm laser source as a direct pump source for ZBLAN based fiber with a dramatic increase in core diameter. The M-type fiber can prove a milestone in the development of all-fiberized high power supercontinuum sources pumped by a low cost 1.55 μm pump source. Furthermore, M-type fibers will offer the advantages of easy fabrication and handling compared to air-hole based photonic crystal fibers.

Methods

In this study, we use finite element method based commercially available software known as COMSOL MULTIPHYSICS for numerical simulations. The effective refractive index of different modes was calculated with respect to wavelength with a step size of 1 nm. A fine mesh of triangular elements with a maximum size of 1 μm was used for entire calculations. The smaller is the mesh size, lower is the error of calculations, however it comes at the cost of computation time. For our calculations, the chosen mesh size is lower than any wavelength operated: mesh size (max) = 1 μm < any operating wavelength between 2 to 10 μm to maintain high standards of calculations. The dispersion, the second order derivative of effective refractive index with respect to wavelength (1), was calculated using finite difference method with a fourth-order accuracy using following expression (2).

$$D_{\lambda} = \frac{-\lambda}{c} * \frac{d^2n}{d\lambda^2}$$

$$D_{\lambda(0)} = \frac{-\lambda_0}{c} * \frac{-2n_{-2} + 32(n_{-1}) - 60(n_0) + 32(n_1) - 2(n_2)}{24\Delta\lambda^2}$$

λ_0 = Operating wavelength, $\Delta\lambda$ = step-size of wavelength, n_{-2} , n_{-1} , n_0 , n_1 , and n_2 are the effective indices at $\lambda - 2\Delta\lambda$, $\lambda - \Delta\lambda$, λ , $\lambda + \Delta\lambda$, and $\lambda + 2\Delta\lambda$ operating wavelength respectively, and c is the speed of light in vacuum.

The unit of Dispersion (D_{λ}) is ps/nm.km, therefore λ is on nm scale and c , speed of light is on km/ps scale.

References

1. Neves, I. V. & Fernandes, A. S. C. Modal characteristics for W-type and M-type dielectric profile fibers. *Microwave and Opt. Techno. Lett.* **22**, 398–405 (1999).
2. Hautakorpi, M. & Kaivola, M. Modal analysis of M-type-dielectric-profile optical fibers in the weakly guiding approximation. *JOSA B* **22**, 1163–1169 (2005).
3. Ghatak, A. K., Goyal, I. C. & Jindal, R. Design of a waveguide refractive index profile to obtain a flat model field. *Proc. SPIE* **3666**, 40–44 (1999).
4. Dawson, J. W. *et al.* Large flattened mode optical fiber for reduction of non-linear effects in optical fiber lasers. *Proc. SPIE* **5335**, 132–139 (2004).
5. Valentin, C. *et al.* Top-hat beam output of a single-mode microstructured optical fiber: impact of core index depression. *Opt. Express* **21**, 23250–23260 (2013).
6. Gerome, F. *et al.* Highly dispersive large mode area photonic bandgap fiber. *Opt. Lett.* **32**, 1208–1210 (2007).
7. Belanov, A. S. & Tsvetkov, S. V. High-index-ring three-layer fibres for mode-locked sub-1.3 μm fibre lasers. *Quant. Electronics* **40**, 160–162 (2010).
8. Aleshkina, S. S. *et al.* Low-loss hybrid fiber with zero dispersion wavelength shifted to 1 μm . *Opt. Express* **21**(20), 23838–23843 (2013).
9. Aleshkina, S. S. *et al.* Quasi-single-mode hybrid fibre with anomalous dispersion in the 1 mm range. *Quantum Electronics* **46**, 738 (2016).
10. Aleshkina, S. S. *et al.* Asymptotically single-mode hybrid fiber for dispersion management near 1 μm . *IEEE J. of Sel. Top. In Quant. Electron.* **24** (2018).
11. Aleshkina, S. S. *et al.* Nonlinear pulse compression in single-mode Yb-doped hybrid fiber with high anomalous dispersion at 1.064 μm . *ASSL. Ath2A.* **4** (2018).
12. Israelsen N. M. *et al.* Real-time high-resolution mid-infrared optical coherence tomography, *Nature: Light Sci and Application*, **11** (2019).
13. Petersen *et al.* Mid-Infrared multispectral tissue imaging using a chalcogenide fiber supercontinuum source. *Opt. Lett.* **43**, 999–1002 (2018).
14. Petersen *et al.* Towards a table-top synchrotron based on supercontinuum generation. *Infrared Phy. & Tech.* 182–186 (2018).
15. Ranka, J. K., Windeler, R. S. & Stentz, A. J. Visible continuum generation in air-silica microstructure optical fibers with anomalous dispersion at 800 nm. *Opt. Lett.* **25**, 25–27 (2000).
16. Dudley, J. M., Genty, G. & Coen, S. Supercontinuum generation in photonic crystal fiber. *Rev. Mod. Phys.* **78**, 1135–1184 (2006).
17. Knight, J. C. *et al.* Anomalous dispersion in photonic crystal fiber. *IEEE Photonics Technology Letters* **12**, 807–809 (2000).
18. Shaw, L. B. *et al.* IR supercontinuum generation in As-Se photonic crystal fiber. Presented at the Conf. Adv. Solid State Lasers (ASSL), Seattle, WA, Paper **TuC5** (2005).
19. Troles, J. *et al.* Low loss microstructured chalcogenide fibers for large nonlinear effects at 1995nm. *Opt. Express* **18**, 26647–26654 (2010).
20. Ebdorff-Heidepriem, H. *et al.* Fluoride glass microstructured optical fiber with large mode area and mid-infrared transmission. *Opt. Lett.* **33**, 2861–2863 (2008).
21. Jiang, X. *et al.* Deep-ultraviolet to mid-infrared supercontinuum generated in solid-core ZBLAN photonic crystal fibre. *Nat. Photonics* **9**, 133–139 (2015).
22. Jain, D. & Bang, O. High power mid-infrared fiber based supercontinuum sources: current status and future perspectives. (Invited) *CLEO Pacific Rim Conference*, **Th3D.5** (2018).
23. Møller, U. *et al.* Multi-milliwatt mid-infrared supercontinuum generation in a suspended core chalcogenide fiber. *Opt. Express* **23**(3), 3282–3291 (2015).
24. Kubat, I. *et al.* Mid-infrared supercontinuum generation to 12.5 μm in large NA chalcogenide step-index fibres pumped at 4.5 μm . *Opt. Express* **22**(16), 4887–4892 (2014).

25. Ramachandran, S. *et al.* Anomalous dispersion in a solid, silica based fiber. *Opt. Lett.* **31**, 2532–2534 (2006).
26. Nicholson, J. W., Ramachandran, S. & Ghalimi, S. A passively-modelocked, Yb-doped, figure-eight, fiber laser utilizing anomalous-dispersion higher-order-mode fiber. *Opt. Express* **15**, 6623–6628 (2007).
27. Dantanarayana, H. G. *et al.* Refractive index dispersion of chalcogenide glasses for ultra-high numerical-aperture fiber for mid-infrared supercontinuum generation. *Opt. Mat. Exp.* **4**, 1444–1455 (2014).
28. Petersen, C. R. *et al.* Mid-infrared supercontinuum covering the 1.4–13.3 μm molecular fingerprint region using ultra-high NA chalcogenide step-index fibre. *Nat. Photonics* **8**, 830–834 (2014).
29. G-Sanchez, I., Ras, D. V. & Birks, T. A. The Airy fiber: an optical fiber that guides light diffracted by a circular aperture. *Optica* **3**, 270–276 (2016).
30. Lægsgaard, J. Gap formation and guided modes in photonic bandgap fibres with high-index rods. *J. Opt. A: Pure Appl. Opt.* **6**, 798–804 (2004).
31. Deng, D. *et al.* Mid-infrared supercontinuum covering 3–10 μm using a As_2Se_3 core and As_2S_5 cladding step-index chalcogenide fiber. *Advanced Solid State Lasers Conference ATu2A* **32** (2015).
32. Cheng, T. *et al.* Mid-infrared supercontinuum generation spanning 2.0 to 15.1 μm in a chalcogenide step-index fiber. *Opt. Lett.* **41**, 2117–2120 (2016).
33. Fortin, V., Bernier, M., Bah, S. T. & Vallee, R. 30 W fluoride glass all-fiber laser at 2.94 μm . *Opt. Lett.* **40**, 2882–2885 (2015).
34. Orsila, L., Sand, J., Narhi, M., Genty, G. & Steinmeyer, G. Supercontinuum generation as a signal amplifier. *Optica* **2**, 757–764 (2015).
35. Gauthier, J. C., Fortin, V., Duval, S., Vallee, R. & Bernier, M. In-amplifier mid-infrared supercontinuum generation. *Opt. Lett.* **40**, 5247–5250 (2015).
36. Swiderski, J. High-power mid-infrared supercontinuum sources: Current status and future perspectives. *Prog. Quantum Electron.* **38**, 189–235 (2014).
37. Jain, D. *et al.* Record power, ultra-broadband supercontinuum source based on highly GeO_2 doped silica fiber. *Opt. Express* **24**, 26667–26677 (2016).
38. Jain, D. *et al.* Scaling power, bandwidth, and efficiency of mid-infrared supercontinuum source based on a GeO_2 -doped silica fiber. *Special Issue on Supercontinuum Generation, JOSA B* **36**, A86–A92 (2018).
39. Islam, M. N. All-fiber designs extend supercontinuum sources into the mid-IR region. *Laser Focus World* **48**, 56–60 (2012).
40. Petersen, C. *et al.* Spectral-temporal composition matters when cascading supercontinua into the mid-infrared. *Opt. Express* **24**, 749–758 (2016).
41. Gan, F. Optical Properties of fluoride glasses: A review. *J. Non-Cryst. Solids* **184**, 9–20 (1995).
42. Kubat, I., Agger, C. S., Moselund, P. M. & Bang, O. Mid-infrared supercontinuum generation to 4.5 μm in uniform and tapered ZBLAN step-index fibers by direct pumping at 1064 or 1550 nm. *J. Opt. Soc. Am. B* **30**, 2743–2757 (2013).

Acknowledgements

The authors acknowledge financial support from Innovation Fund Denmark for the project ShapeOCT (J. No. 4107-00011 A). DJ acknowledges the support from Hans Christian Ørsted COFUNDED Marie-curie action fellowship. DJ acknowledges the support from Hans Christian Ørsted running cost project. DJ acknowledges the support from “The University of Sydney fellowship”. CM acknowledges support from the Danish Council for Independent Research (FTP Case No. 4184-00359B).

Author Contributions

D.J. conceived the idea and implemented the numerical simulations. C.M., A.S. and T.B. judged the fabrication feasibility and are leading the fabrication part of the project. O.B. supervised the project. All authors analyzed the results and reviewed the manuscript.

Additional Information

Competing Interests: The authors declare no competing interests.

Publisher’s note: Springer Nature remains neutral with regard to jurisdictional claims in published maps and institutional affiliations.



Open Access This article is licensed under a Creative Commons Attribution 4.0 International License, which permits use, sharing, adaptation, distribution and reproduction in any medium or format, as long as you give appropriate credit to the original author(s) and the source, provide a link to the Creative Commons license, and indicate if changes were made. The images or other third party material in this article are included in the article’s Creative Commons license, unless indicated otherwise in a credit line to the material. If material is not included in the article’s Creative Commons license and your intended use is not permitted by statutory regulation or exceeds the permitted use, you will need to obtain permission directly from the copyright holder. To view a copy of this license, visit <http://creativecommons.org/licenses/by/4.0/>.

© The Author(s) 2019